Food Research International 221 (2025) 117501

Contents lists available at ScienceDirect

Food Research International

journal homepage: www.elsevier.com/locate/foodres

Online SPME-GC-MS is a feasible method to monitor lipid oxidation during simulated digestion of oils incorporated in a meal

Gabriele Beltrame [1], Kaisa M. Linderborg, Annelie Damerau [*]

Food Sciences, Department of Life Technologies, University of Turku, 20014 Turku, Finland

ARTICLE INFO

Keywords:
Schizochytrium
Simulated digestion
Lipid oxidation
SPME-GC-MS
NMR

ABSTRACT

The clear need for marine n-3 PUFAs has brought attention to *Schizochytrium sp*, one of the few microorganisms approved for the production of edible oil rich in docosahexaenoic acid (DHA). The high concentrations of DHA make the oil highly susceptible to oxidation also in the gastrointestinal tract, which is a known pro-oxidant environment. In the present study, the development of volatile compounds was directly monitored during simulated digestion of *Schizochytrium sp* oil added to a simulated meal, with rapeseed and cod liver oils used as comparison. Volatiles were extracted during the incubation period of subsequent gastric and intestinal phases and directly analyzed with a headspace solid-phase microextraction-gas chromatography–mass spectrometry (HS-SPME-GC-MS) system. Volatile data analysis discriminated all the oils and digestion phases. Total aldehydes, total ketones, and total volatiles areas showed strong correlations with oxidation products in digesta analyzed with proton nuclear magnetic resonance spectroscopy (^{1}H NMR). Our results proved the suitability of our approach for a more comprehensive monitoring of lipid oxidation in simulated gastrointestinal models.

1. Introduction

Marine omega-3 polyunsaturated fatty acids (n-3 PUFAs) such as eicosapentaenoic (20:5n-3, EPA) and docosahexaenoic (22:6n-3, DHA) acids are essential for human health and development (Saini & Keum, 2018). However, their dietary intake, mainly originating from seafood, is inadequate for most of the world population (Micha et al., 2014). While fisheries are globally at or beyond sustainability levels (FAO, 2022), utilization of sidestreams has been considered unable to satisfy global demand (Tocher et al., 2019). Shepon and coworkers, utilizing data elaborated by Hamilton (Hamilton et al., 2020), estimated that the diversion of catch currently used for fish meal and oil production to human consumption, combined with intensification of recycling, would bring current DHA and EPA availability to 45 % of the global demand (Shepon et al., 2022). In addition to this industrial challenge, the ocean DHA production is projected to decline due to the increase in water temperature (Colombo et al., 2020). Therefore, n-3 PUFAs need to be produced *de novo*. Marine thraustochytrids, typically represented by *Schizochytrium sp*, have drawn attention due to their high cell lipid and DHA contents (Demets & Foubert, 2021). Six strains of *Schizochytrium sp* are currently approved by EFSA for the production of oil, which is available on the market and also utilized as ingredient for infant formulas (Cruz & Vasconcelos, 2023).

The nutritional quality of DHA-rich oils is challenged by their proneness to oxidation. Lipid oxidation generates hydroperoxides, which decompose to alkoxy and hydroxy radicals and further rearrange, producing multiple secondary oxidation products with proven bioavailability. At least at low levels, aldehydes, acids, and alcohols derived from lipid oxidation can be detected in blood after ingestion (Schaich, 2020). Of these, aldehydes are particularly reactive and readily form Schiff bases with proteins and DNA, with potential pro-inflammatory and cytotoxic effects (Vieira et al., 2017). Different degrees of oxidation damage have been observed *in vivo*. Ingestion of oxidized oil exfoliated the intestinal brush-border membrane in rats (Kimura et al., 1984), while aldehydes arising from lipid oxidation caused oxidative stress and decreased intestinal immunocompetence in chicken (Liang et al., 2015).

Most n-3 PUFA oxidation studies focus on production and storage conditions, while the oxidative fate of these compounds after ingestion has been less considered. The gastrointestinal tract has pro-oxidant conditions due to the incorporation of oxygen during mastication, the low pH of the stomach, the metal ions present in foods, and the increased

* Corresponding author.
E-mail address: annelie.damerau@utu.fi (A. Damerau).
[1] Present address: Food and Nutrition Sciences, Department of Life Sciences, Chalmers University of Technology, 41296 Gothenburg, Sweden.

https://doi.org/10.1016/j.foodres.2025.117501
Received 22 May 2025; Received in revised form 13 August 2025; Accepted 14 September 2025
Available online 16 September 2025

exposure to oxidants in the micellar phase of lipids in the small intestine (Nieva-Echevarría et al., 2020). In addition, oxidation seems to be influenced by the lipase activity, probably due to decreased steric hindrance from triacylglycerol (TAG) to diacylglycerol (DAG) facilitating exposure to oxidants (Beltrame et al., 2023; Tullberg et al., 2019).

Typically, lipid oxidation is monitored with colorimetric indirect methods such as peroxide and p-anisidine values. However, the earlier might under- or overestimate oxidation due to formation/decomposition during analysis, while the latter lacks specificity. More direct approaches include gas chromatography coupled with mass spectrometry (GC-MS) and proton nuclear magnetic resonance spectroscopy (^{1}H NMR) (Damerau et al., 2020). On the other hand, lipid oxidation in the gastrointestinal tract can be studied utilizing *in vitro* models. The protocol with the widest consensus is INFOGEST 2.0, simulating mouth, stomach, and intestine phases of digestion (Brodkorb et al., 2019). It has been applied to simulate digestion of lipids and to study emulsions and release of hydrophobic molecules of interest (Beltrame et al., 2024; Zhou et al., 2023). However, the application of INFOGEST for the investigation of lipid oxidation during digestion has been more limited and most studies utilized colorimetric methods, while few utilized liquid chromatography coupled to mass spectrometry for analysis of target aldehydes (Nieva-Echevarría et al., 2020; Tullberg & Undeland, 2021).

Nieva-Echevarrìa and coworkers studied the development of primary and secondary oxidation products during simulated digestion of cod liver oil with ^{1}H NMR and headspace solid-phase microextraction (HS-SPME) coupled to GC-MS. In their work, volatile compounds were extracted from the headspace of digesta aliquots after simulated digestion, which was performed according to protocols available prior to INFOGEST 2.0 (Nieva-Echevarría et al., 2017). The aim of the present work was to monitor in untargeted manner the development of volatile compounds during simulated digestion of *Schizochytrium sp* oil in presence of a simulated meal, with cod liver and rapeseed oils as comparison, and to monitor in parallel the progression of oxidation in the digesta with ^{1}H NMR spectroscopy and the progression of tocopherol consumption with liquid chromatography. Differently from previous works, in the present study volatiles were directly extracted from headspace during simulated digestion, which was performed utilizing the chromatographic apparatus as incubation vessel, *i.e.* with an online setup.

2. Materials and methods

2.1. Starting material

All chemical solvents and all salts were supplied by Sigma-Aldrich (Saint Louis, MO, USA) or VWR Chemicals (Leuven, Belgium), respectively, unless specified otherwise. Refined rapeseed, cod liver, and *Schizochytrium sp.* oils were obtained from commercial sources. Hexane solutions of the oils were prepared for dosing equal amounts of oils for digestions and stored at −20 °C prior to experiments. For simulated digestion, rabbit gastric lipase (RGE15-500) was obtained from Lipolytech (Marseille, France), while amylase, porcine pepsin, porcine pancreatin, and bile salts (sodium cholate and sodium deoxycholate) were purchased from Sigma-Aldrich (Saint Luis, USA). For rabbit gastric lipase and pancreatin, 1 U represented 1 μmol of butyric acid released per minute during enzymatic assay performed with tributyrin (Sigma-Aldrich) according to (Grundy et al., 2021). Enzymes were stored according to manufacturer guidelines and bile salts were stored in desiccator. Potato flour, whey protein concentrate, and wheat bran were supplied by Finnamyl Oy (Kokemäki, Finland), HSNG AB (Solna, Sweden), and Raisio Oy (Raisio, Finland), respectively.

2.2. Preparation of simulated meal

A simulated meal was prepared for the online simulated digestion experiments as previously published (Beltrame et al., 2023). Ingredients were not defatted as residual solvents interfered with the SPME-GC-MS analysis in a test run. The simulated meal was prepared by mixing potato flour, whey protein, and wheat bran and heating at 100 °C for 20 min after the addition of deionized water. Simulated meal and the oils were added separately. Total lipid content of the simulated meals was 11.8 % after oil addition. Henceforth, simulated meal without the addition of oil is labeled as SF, while the simulated meals added with rapeseed oil, cod liver oil, and *Schizochytrium sp* oil are labeled as RO, FO, and MO, respectively.

2.3. Fatty acid analysis

The fatty acid composition of oils and of SF was analyzed with gas-chromatography with flame-ionization detector (GC-FID) after methylation. Prior to analysis, lipids were extracted twice from SF, after addition of 4 mL of deionized water, with hexane/isopropanol (2:1, *v*/v) at a 1:1 v/v ratio. Lipids were methylated with a methanolic hydrochloric acid mixture. Triheptadecanoin (Larodan, Solna, Sweden) was used as internal standard. Details of the analysis have been reported elsewhere (Damerau et al., 2020).

2.4. Simulated digestion and online SPME-GC-MS analysis

2.4.1. Simulated digestion

The protocol utilized in this work was adapted from the INFOGEST 2.0 (Brodkorb et al., 2019). The simulated digestion consisted of three subsequent phases, mouth, stomach, and intestine, of which the first lasted two minutes and the others two hours. All digestions were performed in SPME vials. When mouth and stomach phases were performed, only the second was carried online, due to the short length of the first. To have intestinal phase carried online, mouth and stomach phases were carried offline. The mouth and stomach phase combined are labeled as “ms”, while the combination of mouth, stomach, and intestine phases are labeled as “msi”. The salt composition of mouth, gastric, and intestinal fluids was in accordance with INFOGEST 2.0. Optimization of pH with HCl or NaOH 1 mol/L and addition of $CaCl_2$ to the simulated fluids were performed only prior to enzyme addition. Aliquots of acid or base for pH optimization (7, 3, and 7, for mouth, gastric, and intestinal phases, respectively) were determined prior to digestions. Enzyme solutions were prepared the day of the experiments. Incubations, when not performed with the GC-MS autosampler, were performed in a HP GC oven (Hewlett Packard 6890 Series Plus G1530A, Wilmington, DE, USA). Solutions were kept at 37 °C before use in the oven. Simulated saliva contained alfa-amylase 75 U/mL. Simulated gastric fluid contained pepsin and rabbit gastric lipase in amounts to reach enzymatic activity of 2000 U/mL and 60 U/mL in the final chime volume, respectively. Simulated intestinal fluid contained pancreatin and bile salts in amounts to reach lipase activity 2000 U/mL and concentration of 10 mmol/L in the final digesta, respectively.

An aliquot of oil solution in hexane was pipetted in a SPME vial previously flushed with nitrogen to obtain 120 mg of oil. After vigorous nitrogen flushing in the dark for 30 min to remove the hexane, simulated food (about 0.9 g) was added to the vial. To start simulated digestion, simulated saliva was added to the vial and a glass rod was used to simulate chewing by hitting the mixture 32 times. The vial was incubated for 2 min at 37 °C in the HP GC oven. Simulated gastric fluid was quickly added to the SPME vial, which was subsequently placed in the GC-MS autosampler to start the incubation and analysis. While the GC-MS carried out the incubation and SPME of the gastric phase, another mouth and gastric phases were simulated in the HP GC oven. To facilitate the start of the online intestinal phase, the online gastric phase ended before the end of the offline gastric phase. At the end of the latter, simulated intestinal fluid were quickly added to the SPME vial, which was placed in the autosampler for immediate incubation and analysis. Each digestion phase (ms or msi) was performed in triplicate.

2.4.2. SPME-GC-MS analytical conditions

Thermo Scientific GC-MS instrument consisted of TriPlus RSH autosampler (Waltham, MA, USA) and a Trace 1310 GC connected to ISQ 7000 mass spectrometer (ThermoFisher) and equipped with SPB-624 capillary column (60 m × 0.25 mm × 1.4 μm, Supelco, Bellefonte, PA, USA). The fiber employed for HS extraction was DVB/CAR/PDMS 50/30 μm (Supelco, Bellefonte, PA, USA). SPME vials were incubated for 1.5 h at 37 °C at 250 rpm agitation (with switching directions every 10 s) and extracted for 30 min at the same incubation conditions, for a total duration of online gastric and intestinal phases of 2 h, in accordance with INFOGEST 2.0. Desorption (5 min) temperature in GC-injector port was 240 °C (splitless injection) and column temperature: 40 °C held for 6 min, 5 °C/min to 200 °C, held for 10 min. Helium (1.4 mL/min) was used as carrier gas. Electron ionization at 240 °C and 70 eV was employed for the MS and mass to charge ratios were scanned between 40 and 300 amu. Instrument parameters for the analysis of lipid oxidation products were optimized previously (Damerau et al., 2020). Alkane standards (C7–C30, Supelco, Bellefonte, PA, USA) were used for retention index (RI) calculation. Compound identification was based on relative match (RMatch) of mass fragmentation with NIST MS Search library (version 2.4, National Institute of Standards and Technology, Gaithersburg, MD, USA) and on comparison of experimental RI and tabulated RI. Acquired data was processed by Chromeleon 7.2.9 Chromatography Data System (Thermo Fisher Scientific, Waltham, MA, USA).

2.4.3. Lipid extraction from digesta

At the end of the HS-SPME extraction and after injection in the GC-MS system, each SPME vial was immediately put on ice and lipids were extracted as previously described (Beltrame et al., 2023) and stored at −80 °C.

2.5. ^{1}H NMR analysis

^{1}H NMR spectra were collected from oils and lipids extracted from digesta. For the analysis, 500 μL of sample was dried with N_2 flow and recollected to 200 μL of $CDCl_3$, of which 180 μL was pipetted into 3 mm NMR tubes. ^{1}H NMR spectra were collected at 298 K with a Bruker Avance 600 MHz (Bruker Biospin, Switzerland) equipped with a Prodigy TCI CryoProbe and SampleJet sample changer. Proton spectra were collected with 32 scans, an acquisition time of 4 s, and a relaxation time of 5 s (Ahonen et al., 2022). NMR data were processed with TopSpin 4.0.7 (Bruker, MA, USA).

2.6. Tocopherol analysis

Tocopherols were quantified in the different samples and lipids extracted from digesta utilizing a Shimadzu Nexera XR LC-30 system equipped with RF-20A fluorescence detector (292–325 nm excitation-emission wavelengths) and a Phenomenex OOG-4162-EO Luna 3 μm silica column (Aitta et al., 2023). The mobile phase was heptane:1,4-dioxane 98:2 *v*/v used without gradient. Column was kept at 30 °C, while the autosampler was kept at 4 °C. Tocopherol standard curves were prepared using α-, β-, γ-, and δ-tocopherol stock solutions. Undigested oils were diluted in heptane, while digestates were filtrated with 0.45 μm PTFE filters, dried with N_2 at room temperature in dim light and recovered with heptane. Chromatographic data was processed with the software LabSolutions 5.93 (Shimadzu Corporation, Kyoto, Japan). Tocopherol concentrations are reported as ng/mg of oil or lipid extract from digesta.

2.7. Statistical analysis

The statistical analysis was performed with RStudio (RStudio., 2020). Shapiro-Wilk and Levene tests (*dlookr* and *car* packages) were used to assess normality of the data and homogeneity of data variance. The analysis of variance was performed with the functions *aov* and *TukeyHSD* (*stats* package) for ANOVA test or oneway for Games-Howell posthoc test (*userfriendlyscience* package). In rejection of normality, Kruskal test was performed with *kruskal.test*, followed by *pairwise.wilcox.test* (*stats* package). The confidence level of 95 % ($p < 0.05$) was used for statistical significance. Pearson and Spearman correlation coefficients were calculated with *correlation* function (*correlation* package).

Principal component analysis (PCA) of logarithm-transformed and Pareto-scaled SPME-GC-MS data was performed with *FactoMineR* package. The most important loadings of the obtained PCA model were selected according to their contribution values (*fviz_contrib* function of *factoextra* package). Contribution cutoff was the reverse number of compounds used to compute the PCA model. Variable correlations with principal components and their respective *p*-values were computed with *dimdesc* function (*FactoMineR* package). Partial least squares-discriminant analysis (PLS-DA) of the logarithm-transformed, mean-centered, and Pareto-scaled SPME-GC-MS data was performed with *ropls* package (Thévenot et al., 2015). Modelled responses were digestion phases, sample class, and discrimination between absence and presence of oil. Cross-validation, confusion test, and VIP values were computed with the same package.

3. Results and discussion

3.1. Fatty acid and tocopherol composition of samples

The fatty acid composition of the oils utilized in this study has been analyzed with gas chromatography. The complete composition has been reported elsewhere (Beltrame et al., 2025). Briefly, rapeseed oil contained (*w*/w%) 18:1n-9 (61.9 %) and 18:2n-6 (18.4 %), *Schizochytrium sp* oil contained 22:6n-3 (45.7 %), 16:0 (19.8 %), and 14:0 (9.9 %), and cod liver oil contained 18:1n-9 (15 %), 20:1n-9 (14.5 %), 22:6n-3 (13.4 %), and 20:5n-3 (9.9 %). The lipid content of SF was about 0.1 %. Its main fatty acids were (w/w%) 18:1n-9 (28.9 %), 16:0 (27.8 %), and 18:2n-6 (10.4 %). The tocopherol content of *Schizochytrium sp* oil differed noticeably from rapeseed and cod liver oils, as the total content was respectively 7 and 9 times higher. Also, it mainly consisted of γ- (62 w/w%) and δ- (25 w/w%) tocopherols, while rapeseed and cod liver oils mainly had α- and γ-tocopherol in close amounts (α/γ w/w ratio of 0.8 and 0.6, respectively) (Table 1).

Differences in tocopherol concentration were observed between oil

Table 1
Tocopherol content of undigested and digested oils. Different letters mark significant differences between samples ($p < 0.05$).

	Tocopherol (ng/mg)				
	α-	β-	γ-	δ-	total
RO	197.0 ± 11.6b,c	1.0 ± 0.0c	262.8 ± 13.6c	4.2 ± 0.5c	464.9 ± 25.6c
ROms	193.4 ± 32.4b,c	1.3 ± 0.3c	253.9 ± 55.6c	6.1 ± 1.5c	454.6 ± 59.6c
ROmsi	181.2 ± 18.7c,d	1.2 ± 0.2c	237.4 ± 23.8c	5.5 ± 0.3c	425.2 ± 42.9c
MO	357.7 ± 5.4a	65.1 ± 1.7a	2022.7 ± 63.7a	806.0 ± 24.6a	3251.5 ± 95.0a
MOms	258.8 ± 27.5b	41.1 ± 5.4b	1301.9 ± 155.5b	491.0 ± 58.1b	2092.8 ± 246.4b
MOmsi	256.9 ± 55.0b	38.1 ± 7.3b	1230.2 ± 246.4b	468.6 ± 95.8b	1993.8 ± 404.3b
FO	110.6 ± 3.0d,e	4.0 ± 0.1c	180.6 ± 1.4c	80.7 ± 2.7c	375.9 ± 5.4c
FOms	72.1 ± 5.3e	3.4 ± 0.4c	141.1 ± 8.2c	66.0 ± 4.3c	282.6 ± 16.1c
FOmsi	66.1 ± 11.2e	3.6 ± 0.1c	132.8 ± 7.3c	60.8 ± 0.4c	263.3 ± 18.6c

RO: rapeseed oil; MO: *Schizochytrium sp* oil; FO: cod liver oil; ms: mouth+gastric; msi: mouth+gastric+intestine.

digesta and the respective undigested oils. For RO, the differences lacked statistical significance. The observed decreases in FO, such as the average α-tocopherol decrease of 35 % and 40 % after ms and msi phases, respectively, and the average γ-tocopherol decrease of 22 % and 26 %, respectively, lacked statistical significance. *Schizochytrium sp* oil, on the other hand, had γ-tocopherol average losses of 36 % and 39 % after ms and msi phases, respectively, and δ-tocopherol average losses of 39 % and 42 % after ms and msi phases, respectively. The differences between MOms and MOmsi lacked significance (Table 1). Therefore, FO hinted and MO showed that most of the tocopherol loss during simulated digestion can be attributed to the stomach phase. Radical scavengers were reported by Lorrain and coworkers to efficiently prevent lipid oxidation in sunflower oil at simulated gastric conditions. Such activity decreased when same experiments were conducted with *ex vivo* gastric juice. Authors ascribed such loss of activity to the higher presence of protein in the digestion medium (Lorrain et al., 2012). Therefore, it is

Table 2
Volatile compounds identified in the HS-SPME-GC-MS analysis. The identification of the compounds is based on their mass fragmentation and retention index (RI).

Compound	RT	NIST Rmatch	RI NIST (polar column)	RI experimental	Specific presence in samples*
acid					
butanoic acid	29.61	973	1624 ± 11	1643	
pentanoic acid	34.36	876	1733 ± 13	1761	
hexanoic acid	38.21	924	1846 ± 12	1863	
octanoic acid	44.67	904	2060 ± 15	2080	
nonanoic acid	47.38	879	2170 ± 17	2141	
decanoic acid	49.49	881	2276 ± 15	2228	
alcohol					
2-propanol	6.7	888	926 ± 15	936	msi
2,4-dimethyl-1-heptanol	9.02	785	1030 ± 41	1031	SFmsi
1-butanol	12.6	938	1142 ± 11	1152	SF
3/4-methyl-2-pentanol	13.22	890 / 920	1181 ± 21 / 1168 ± 4	1171	msi
3-hexanol	14.08	880	1198 ± 9	1197	MOms, FO
1-pentanol	15.73	940	1250 ± 9	1255	
1-hexanol	18.93	907	1355 ± 7	1359	
1-octen-3-ol	22.15	964	1450 ± 7	1454	
1-heptanol	22.44	800	1453 ± 9	1461	RO
2-ethyl-1-hexanol	23.7	954	1491 ± 5	1495	
1-octanol	26.52	902	1557 ± 8	1567	
2-octen-1-ol	28.91	833	1613 ± 7	1625	
aldehyde					
3-methyl-butanal	6.36	839	918 ± 7	919	MOmsi, SF
hexanal	10.4	956	1083 ± 8	1078	
2-butyl-2-heptenal	11.79	843	1123 ± 7	1125	SFmsi
heptanal	13.51	873	1185 ± 9	1180	MOms, SF
octanal	16.72	911	1289 ± 9	1287	
2-heptenal	17.92	917	1322 ± 9	1327	FO, SF
2-ethyl-2-hexenal	18.29	864	1333 ± 3	1339	RO, SF
nonanal	20.08	919	1391 ± 8	1394	
2-octenal	21.46	902	1429 ± 8	1434	RO, SF
decanal	23.91	864	1498 ± 8	1500	RO, SFms
benzaldehyde	25.03	921	1520 ± 14	1530	
2-nonenal	25.47	940	1534 ± 10	1541	
undecanal	28.23	853	1604 ± 9	1608	FOms
2-decenal	30.02	913	1644 ± 11	1653	SF
alkene					
2,4-dimethyl-1-heptene	5.69	921	885 ± N/A	882	MO
ester					
isopropyl acetate	5.98	843	900 ± 14	900	FOmsi, SFmsi
butyl butanate	14.57	892	1220 ± 8	1214	SFms
furan					
2-ethyl-furan	7.1	899	951 ± 6	954	SFms
2-pentyl-furan	15.27	942	1232 ± 9	1239	
2-butyl-furan	27.28	818	–	1585	SF
2-furanmethanol	30.82	911	1661 ± 9	1672	SF
2(5H)-furanone	34.58	927	1743 ± 23	1766	RO, SF
ketone					
2-butanone	6.05	863	907 ± 12	904	SFms
3-hexanone	9.59	939	1053 ± 5	1051	MO, FO
4-methyl-2-heptanone	14.2	840	1206 ± 0	1200	ROmsi
4,6-dimethyl-2-heptanone	15.33	904	1262 ± N/A	1241	MO, SF
2-octanone	16.68	921	1287 ± 8	1286	msi
6-methyl-5-hepten-2-one	18.3	822	1339 ± 9	1339	
4-hydroxy-4-methyl-2-pentanone	19.37	827	1358 ± 14	1372	MO, SFms
2-nonanone	20	885	1390 ± 7	1391	
3-octen-2-one	20.71	837	1396 ± 4	1412	ROmsi, SFmsi
2-methyl-3-nonanone	21.05	801	1415 ± N/A	1422	MO
2-decanone	23.83	840	1493 ± 5	1498	ROmsi, SF
3-nonen-2-one	24.63	892	1515 ± 6	1520	SFmsi
2-undecanone	28.04	862	1598 ± 7	1603	
2-tridecanone	36.6	871	1809 ± 6	1782	SFmsi

* SF: observed only in absence of oil; MO: observed only in presence of *Schizochytrium sp* oil; FO; observed only in presence of cod liver oil; RO; observed only in presence of rapeseed oil; ms: observed only during simulated gastric phase; msi: observed only during simulated intestinal phase. Unspecified compounds were ubiquitous or lacked clear trends in their presence in samples. See Section 3.2 for detailed discussion.

possible that the increase in protein content from ms to msi due to the pancreatin addition has influenced the consumption of tocopherol during the intestinal phase.

3.2. SPME-GC-MS analysis

The study of the headspace of the digesta with SPME-GC provided information on the specific nature of volatile compounds generated during the simulated digestion process of RO, MO, FO, and SF only. Analysis of SF indicated volatiles originating from other sources than added lipids. Differently from previous reports, the protocol developed in our laboratory allowed the separated analysis of gastric and intestinal phases of digestion. A total of 54 compounds was identified with NIST library using their mass fragmentations and retention indexes in relation to the alkane standards. Nieva-Echevarrìa was able to identify about 50 compounds in the digesta of cod liver oil employing the NIST library, in addition to the about 30 standards utilized, but they had digested about 4 times more oil (Nieva-Echevarría et al., 2017). Differences in the number of identified volatiles can be ascribed to different oil amounts and oxidation status, but also to the presence of more equilibria of volatile compounds in the vial in addition to the typical oil-headspace-extraction fiber, for example due to the presence of micelles in the intestinal phase.

The overall quality of identification was good. The median library match was 892 and the median deviation from the library RI was 0.3 % (Table 2). The logarithm-transformed peak areas of all volatile compounds were submitted to principal component analysis to identify compounds most relevant for discrimination. Score and loading plots are reported in Fig. 1. The first principal component (34.5 % of variance) separated the SF samples from the others, while the second (20 % of variance) separated MO samples from RO, placing FO in between. The analysis markedly separated msi and ms phases. All msi phases shifted, compared to their respective ms phases, towards the positive side of PC1 and towards the negative side of PC2 (Fig. 1).

Main contributors of PC1 were 1-butanol, 2-decanone, 2-furanmethanol, 2-decenal, and 2-butylfuran, while main contributors of PC2 were 1-octanol, 1-hexanol, 4,6-dimethyl-2-heptanone, 1-heptanol, and 4-hydroxy-4-methyl-2-pentanone (Fig. 1 and **Supplementary Table 3**). According to the cutoff contribution value of 1.85 % (1/54), 32 compounds (2 acids, 7 alcohols, 8 aldehydes, 1 alkene, 3 furan derivatives, and 11 ketones) were relevant for the separation of the samples observed in the score plot. A hierarchical cluster analysis of their log-transformed peak areas is reported in **Supplementary Fig. 1**. As in other analysis, SF separated from the oil samples, RO separated from the marine oils, and finally that MO separated from FO. **Supplementary Fig. 1** shows that seven compounds can be used for the discrimination of the oil-containing digesta. Of these, five compounds were responsible for the discrimination of the marine oils, with two of these produced only by MO, while two volatiles were observed only in RO. The FO and MO samples were discriminated by the production of 3-hexanol and 3-hexanone, which can be ascribed to the lipid oxidation of DHA (Ahonen et al., 2022). The MO samples were discriminated by the production of 2,4-dimethyl-1-heptene, 2-methyl-3-nonanone, and, to a lesser extent, 4-hydroxy-4-methyl-2-pentanone. These volatiles could originate from the degradation of terpenes such as carotenoids or squalene (Shimizu et al., 2018; Sommerburg et al., 2003) or, in case of the latter, branched fatty acids, which can be found in marine microorganisms (Lang et al., 2011) but could be also ascribed to catabolism of branched amino acids (Morabito et al., 2019). The RO samples were discriminated by 1-heptanol, which can be ascribed to the degradation of 11-OOH of n-9 fatty acids (Frankel, 1983), and 4-methyl-2-heptanone, a volatile that has been previously correlated to milk fat (Sabikun et al., 2021). The blank was discriminated by furan derivatives (2-furanmethanol and 2-butylfuran) and by 2-decenal (main contributors of PC1, Fig. 1), the later ascribable to decomposition of 9-OOH of oleic acid (Frankel, 1983).

The peak areas of the most relevant compounds for oil discrimination are reported in Fig. 2. In RO samples, 1-heptanol production was slightly higher during msi than ms phase, while 4-methyl-2-heptanone was observed only during msi phase. In MO samples, 4-hydroxy-4-methyl-2-pentanone was mainly detected with low areas during ms phase. Alkenes and ketones solely observed in MO samples had similar areas between ms and msi phases. On the other hand, the volatiles in common between MO and FO samples had noticeable differences in area, as 3-hexanol arose from both FO samples and was more abundant, compared to MOms, while 3-hexanone was produced slightly more in MO samples than FO (Fig. 2). Interestingly, Nieva-Echevarrìa and coauthors also noticed higher areas of 3-hexenol compared to 3-hexenone after cod liver oil digestion. After different additions of BHT, both volatiles decreased and 3-hexenone disappeared at the highest dosage (Nieva-Echevarría et al., 2017).

Hammer and Schieberle have ascribed alcohol formation from n-3 fatty acids to radical scission after addition of hydroperoxides to neighboring double bonds and have assigned the formation of the corresponding ketone to auto- or enzymatic oxidation (Hammer &

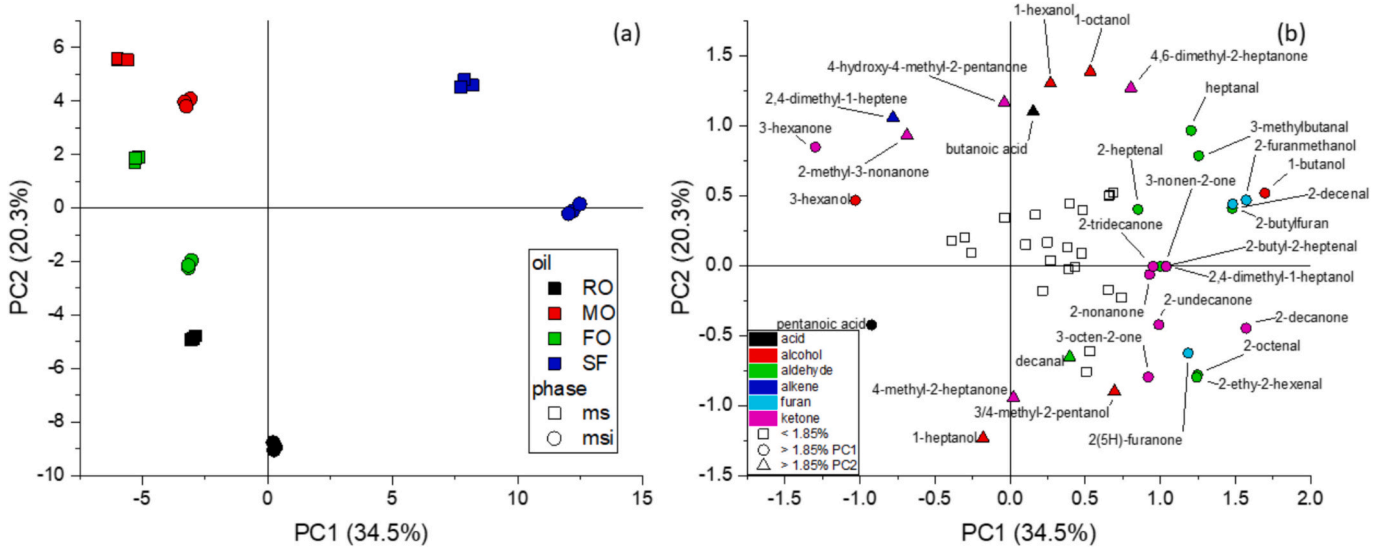

Fig. 1. Scores (a) and loadings (b) obtained from the principal component analysis of the SPME-GC-MS data. Unlabeled loadings have a contribution lower than cutoff (1.85 %).

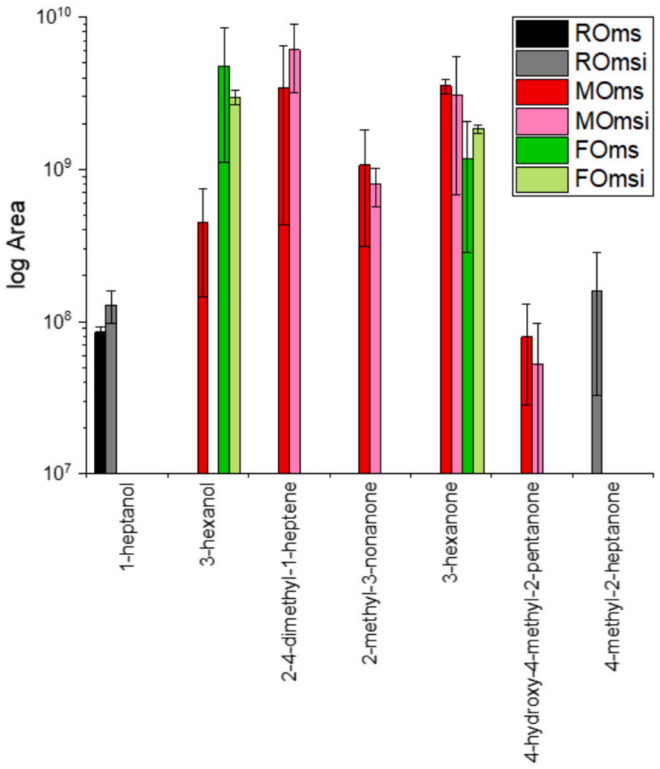

Fig. 2. Peak area values (in logarithmic scale) of volatile compounds relevant for the discrimination of samples added with rapeseed (RO), *Schizochytrium sp* (MO), and cod liver (FO) oils. Values are average ± standard deviation ($n = 3$).

Schieberle, 2013). Therefore, we could speculate that 3-hexanol would likely be produced first and then oxidized to 3-hexanone in the gastrointestinal environment. We could ascribe the oxidation of 3-hexanol in MOmsi to 3-hexanone to the formation of micelles during the intestinal phase, as these would include 3-hexanol due to its poor water solubility and therefore increase its exposure to oxidation. As MO and FO were digested with the same concentration of bile salts, the composition of MO likely interplayed in the phenomenon. It is possible that oxidized tocopherols acted as 3-hexanol oxidants through tocopherol regeneration (Rietjens et al., 2002). Tocopherol regeneration is a known phenomenon at lipid-water interfaces during oxidation (Hennebelle et al., 2024). The pro-oxidant effect would be hinted by the comparison of tocopherol consumption rates in samples and the area of 3-hexanol, which showed, with the exception of α- and β-tocopherol, clear linear trends (Fig. 4a) with adj. R^2 up to 0.958 for δ-tocopherol. A summary of linear and non-parametric correlations is reported in **Supplementary Table 1**. Spearman ρ between 3-hexanol and tocopherol consumption was especially high with δ- (0.97) and γ-tocopherol (0.85). Therefore, the more tocopherol was consumed (*i.e.* oxidized) during simulated digestion, the less 3-hexanol was observed, as oxidized tocopherol would be reduced by 3-hexanol and its respective ketone would be formed.

Scores and loading plots of a PLS-DA model discriminating ms and msi phases are shown in **Supplementary Fig. 2**. The available data produced a good model (R2Y 0.988, Q2Y 0.963, no misassignments in confusion test, **Supplementary Table 2**) in which ms and msi were discriminated by the first component (20.2 %; 86.0 %) and oil-added samples were separated from SF by the second component (28.9 %, 9.5 %). The second component mostly discriminated MO samples from the others, particularly from SF samples. The areas of the top 20 % compounds with VIP > 1 are reported in Fig. 3. Among the compounds, 2-octanone had the highest VIP score (2.93, **Supplementary Table 2**). This volatile correlated with msi phases. The second most relevant compound for discrimination was 3/4-methyl-2-pentanol, which was found in FOmsi, ROmsi, and, with high deviations, in SFmsi. This compound most likely originates from the whey protein included in the simulated food (Frétin et al., 2022). The ketones 2-decanone and 3-octen-2-one were observed mainly in ROmsi and SFmsi, the earlier with high deviations in ROmsi and the latter in SFmsi. Octanal was more abundant in FOmsi, followed by ROmsi, and found with high variance in MO samples, but it was markedly more abundant in SFmsi, compared to all the samples. Nieva-Echevarrìa has described 2-octanone and 3-octen-2-one as originating from digestion blank, but ascribed octanal to oils (Nieva-Echevarría et al., 2017). Volatiles with eight carbons can be ascribed to degradation of DHA (Ahonen et al., 2022) but also of oleic and linoleic acids (Frankel, 1983). Besides correlation with msi, and therefore with a prolonged exposure to pro-oxidant environment, the data presented here can raise a question of a correlation between

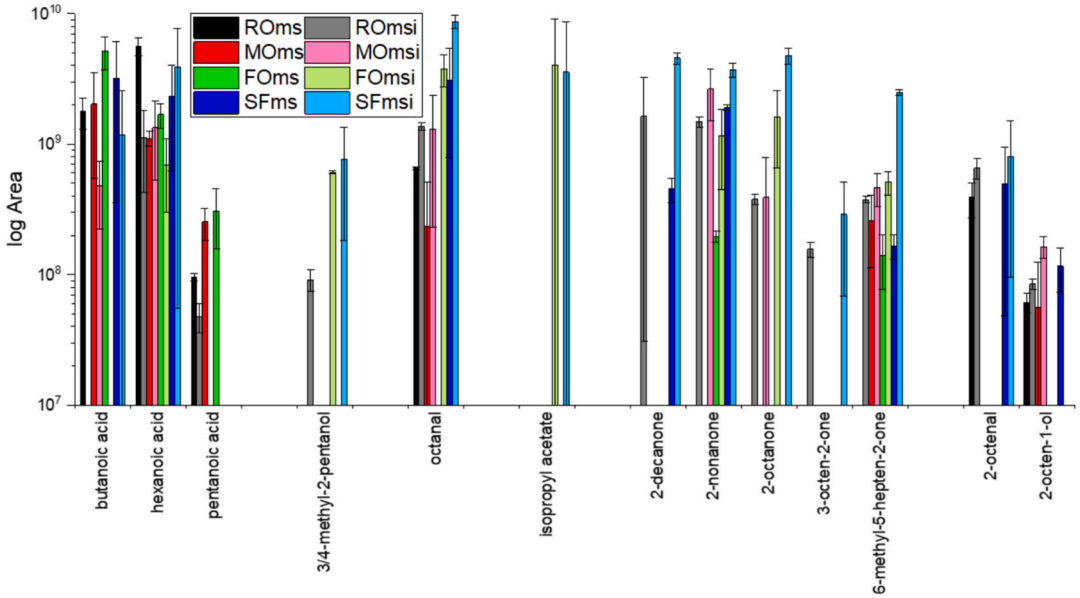

Fig. 3. Peak area values (in logarithmic scale) of volatile compounds relevant for the discrimination of mouth+stomach (ms) and mouth+stomach+intestine (msi) digestion phases of samples added with rapeseed (RO), *Schizochytrium sp* (MO), and cod liver (FO) oils. Values are average ± standard deviation (n = 3).

digestion process and octanal production. The ms phases correlated with the volatile saturated acids. Among them, only the pentanoic acid, produced in the lowest amounts, arose solely from oil-added samples, particularly FOms and MOms. Butanoic acid was found prevalently in FOms and its production in SFms and SFmsi had high deviation. On the other hand, hexanoic acid was ubiquitous among the samples (Fig. 3). Nieva-Echevarrìa assigned hexanoic acid as originating from cod liver oil even though hexanal was irrelevant for discrimination in both their and our studies (Nieva-Echevarría et al., 2017).

A further PLS-DA model was computed to classify the samples according to the added oil, *i.e.* to discriminate RO, MO, FO, and SF. Scores and loading plots are reported in **Supplementary Fig. 3**. The available data produced a model with lower quality compared to the previous one (R2Y 0.996, Q2Y 0.991, but RO was misassigned in confusion test, **Supplementary Table 2**) in which SF samples were discriminated from MO and FO by the first component (35.4 %; 32.8 %) with RO samples situated at the center of p1. The model highlights the volatiles 2-octenal and 2-octen-1-ol. 2-octenal was found in RO and SF with similar areas and slightly more abundant in msi. On the other hand, 2-octen-1-ol was found in RO, MOmsi, and SFms. The higher presence of 2-octen-1-ol in MOmsi but absence in FO samples could be attributed to the degradation of 22:5n-6 (about 8 % *w*/w), as this compound is attributed to oxidation of n-6 fatty acids (Al-Dalali et al., 2022; Kakuta et al., 2013).

Overall, the production of volatiles had negative correlation with the consumption of tocopherols during digestion, indicating a general antioxidant effect. The most visible trends are reported in Fig. 4b-d, which shows the reduction of α-, γ-, and total tocopherols in relation to formation of ketones, aldehydes, and total volatiles. Lower consumption of α-tocopherol had negative effect on ketone formation, while decrease of γ- and total tocopherols affected positively the total amount of volatiles. A clear negative effect of total tocopherols on aldehyde production was absent (Fig. 4b-d). This absence might be due to the high development of these volatiles, particularly benzaldehyde, from the simulated food. It has been reported already that the anti- or pro-oxidant effect of radical scavengers during simulated digestion depends on the oxidation marker considered, in addition to food type, molecular class, and concentration (Nieva-Echevarría et al., 2020). For example, in the study of Martini on turkey meat digestion, the utilization of TBARS as oxidation marker indicated anti-oxidant effect of phenolic compounds in the gastrointestinal tract, but the analysis of hydroperoxides showed marked increases (Martini et al., 2018). In another study on simulated digestion of meat, α-tocopherol had scant antioxidant effect according to malondialdehyde concentration (with even slight increase of the oxidation product at higher concentration), while it neatly prevented hexanal formation (Van Hecke et al., 2016). In this sense, the advantage of our untargeted approach is clear, as it allowed the visualization of

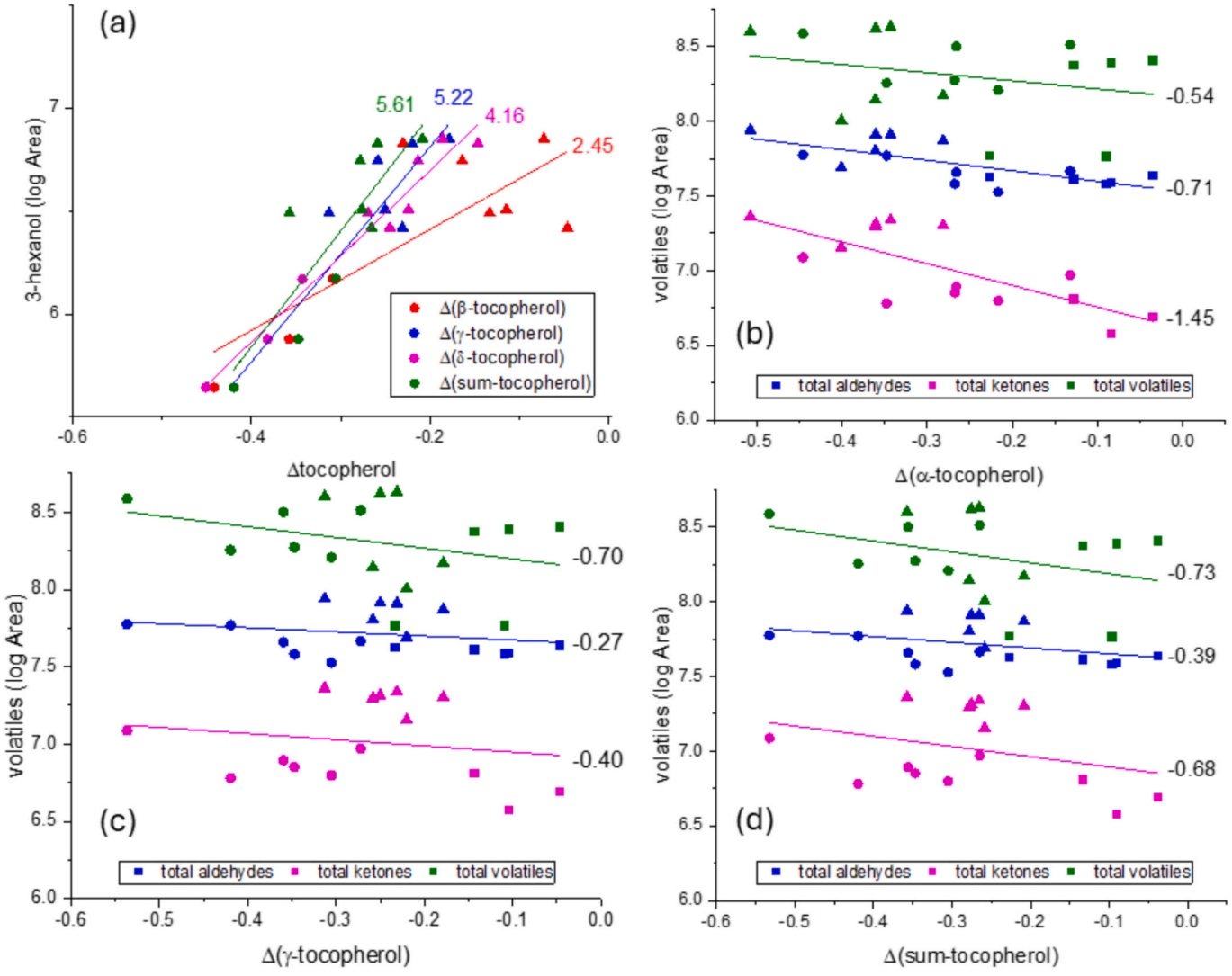

Fig. 4. (a) Relationship between 3-hexanol area (logarithmic scale) and tocopherol consumption. (b,c,d) Relationship between total area of aldehydes, ketones, and all volatiles (logarithmic scale) and α-, γ-, and total tocopherol consumption, respectively. Numbers in the figures indicate the slope of the adjacent line.

multiple volatile species at the same time and identify anti- and pro-oxidant effects.

3.3. ^{1}H NMR analysis

High resolution ^{1}H NMR was applied to the lipid extracts of RO, MO, and FO digesta to study their lipid profiles in an untargeted manner (**Supplementary Fig. 4**). A typical TAG signal pattern was observed, with the *sn*-1/3 and sn-2 position signals around 4.14, 4.29, and 5.24 ppm, respectively. In digesta, signals for di- and monoacylglycerols (DAGs and MAGs) were observed, in particular for 1,2-DAG (3.73, 4.32, and 5.08 ppm), 2-MAG (3.83 and 4.93 ppm), and 1-MAG (3.65, 3.94, and 4.23 ppm). The pattern in the formation of digestion products is explained by the stereoselectivity of the rabbit gastric lipase (ms phase) for *sn*-3 position and of pancreatic lipase (msi phase), which hydrolyses both *sn*-3 and *sn*-1 positions (Rogalska et al., 1990). The presence of 1-MAG can be explained as rearrangement of 1,2-DAG to 1,3-DAG and subsequent hydrolysis of *sn*-1/3 position. The collection of ^{1}H spectra of digesta from both ms and msi phases highlighted the trend in formation of digestion products, which is visible in the relative proton area data reported in **Supplementary Fig. 5a**. As expected, TAGs were mainly hydrolyzed during the intestinal phase. The order of digestibility of the oils was approximately RO > FO ≥ MO, which was in agreement with our previous findings (Beltrame et al., 2025). The final TAG decreases were 34 ± 7 %, 23 ± 9 %, and 27 ± 5 %, respectively. The lower hydrolysis of *Schizochytrium sp* oil can be attributed to the presence of DHA in positions *sn*-1,3 of the TAG molecule (Beltrame et al., 2023). The TAG hydrolysis result of RO, which was lower than the amount reported by Nieva-Echevarrìa for cod liver oil (about 75 %), was actually in agreement with the lipolysis capability of INFOGEST 2.0 protocol, as can be noticed by comparing our values with the power trend of rapeseed oil hydrolysis visible in Sabet and coworkers (Sabet et al., 2022). Tullberg and coworkers showed that in simulated digestion of cod liver oil an increase in lipase amount determined an increase in secondary oxidation products, while inhibition of lipolysis decreased the concentration of these compounds in digesta (Tullberg et al., 2019). More recently, we have noticed that hydroperoxidation of DHA and particularly EPA located in position *sn*-2 of TAGs was easier after hydrolysis of *sn*-1,3 positions in simulated digestion (Beltrame et al., 2023). Despite the evidence, lipolysis is seldomly monitored during simulated digestion in studies focusing on lipid oxidation (Tullberg & Undeland, 2021). Simulated digestion, although simpler than *in vivo* studies, is a complex system, from which it is difficult to extract unambiguous evidence of correlation between lipolysis and lipid oxidation. The complexity is further increased by the required compromise between sample amount and lipolysis degree in experimental designs (Tan et al., 2020). As our work had an untargeted approach, we believe to have reached a good compromise between monitoring of lipid oxidation through HS-SPME-GC-MS and lipid digestion according to INFOGEST 2.0.

Proton signals ascribable to primary oxidation products were found in the 5.6–6.6 ppm region (insert of **Supplementary Fig. 4**). The signals were assigned to conjugated diene systems associated with the hydroperoxide moiety in which each C=C could take either *Z* or *E* configuration. Signals at 5.51 ppm, 5.98 ppm, and 6.48 ppm were assigned to *ZE* configuration, while signals at 5.64 ppm and 6.08 ppm were assigned to *EE* configuration. The signal at 6.44 ppm could be assigned to both *ZE* and *ZZ* (Martínez-Yusta et al., 2014). The signal at 5.81 ppm found only in cod liver oil could be assigned to both position α of hydroperoxyl groups in conjugated double C=C systems (Gardner et al., 1978) and n-1 fatty acids (Fiori et al., 2012). Singlets at 6.37 ppm and 5.73 ppm were assigned to protons in conjugated triene (shortly, C=C=C) systems (Lafountain et al., 2013). The presence of C=C=C could be also ascribed to terpenes, whose oxidative degradation would explain the formation of the branched volatile compounds (Section 3.2). The integration of the normalized signals is reported in **Supplementary Fig. 5b**. The signals of *ZE&EE* protons had the highest intensity in the observed region. Lipid oxidation signals had noticeably lower intensity in RO samples compared to FO and MO samples, although the *ZE&EE* ^{1}H area doubled from ROms to ROmsi, indicating hydroperoxides formation during intestinal phase of digestion. In FO samples, the *ZE&EE* ^{1}H area increased about 40 %, while the C=C=C&n-1 ^{1}H area almost doubled. At the same time, the increase in C=C=C (5.73 ppm) ^{1}H area was marginal, and no changes were observed in *Z(E/Z)&ZE* signals at 6.44 and 6.48 ppm. Typically, hydroperoxide formation in PUFAs implicates rearrangement of double bond position, producing conjugated dienes. Triene hydroperoxides are formed to lower extents, as they require the formation of another bisallylic radical and the formation of a second hydroperoxyl group (Frankel, 2005). The positions of hydroperoxide moieties in DHA chain observed in *Schizochytrium sp* oil are capable of generating conjugated trienes but the required second hydroperoxyl group was absent in our previous simulated digestion study (Beltrame et al., 2024). Differently from FO and RO samples, no statistically significant differences in lipid oxidation signals were observed between ms and msi phases of MO, although both *Z(E/Z)&ZE* and *ZE&EE* ^{1}H areas had noticeable deviations. The observed stabilization of hydroperoxides is the likely result of radical quenching performed by tocopherols and terpenes in the MO samples, which would in turn provide the tocopherol quinone for the oxidation of other molecules (Section 3.2).

3.4. Correlation between ^{1}H NMR signals and volatiles

Pearson correlations between the integration values of the ^{1}H NMR signals discussed in Section 3.3 and the sum of the volatile peak areas are presented in Fig. 5a, while Fig. 5b reports trends among variables with relevant correlations. The total volatile area had strong correlations only with the signals of conjugated dienes ($r = 0.78$ and 0.48). The absence of correlations between total furans area confirmed these volatiles arose mainly from the simulated food (**Supplementary Fig. 1**). The total alcohol area correlated solely with the total sum of volatiles ($r = 0.83$). The total aldehyde area had strong positive correlations with C=C=C signals at 5.73 ppm and 5.81 ppm ($r = 0.81$) but a strong negative correlation with C=C=C signal at 6.37 ppm ($r = -0.78$). The total ester area had a similar but weaker pattern ($r = 0.65$ and -0.63, respectively). The total ketone area had as well positive correlations with triene signals at 5.73 and 5.81 ppm ($r = 0.54$), in addition to strong correlations with conjugated diene signals at 5.98 and 6.08 and 6.44 and 6.48 ppm ($r = 0.89$ and 0.69), noticeably absent with total aldehydes ($r = 0.42$ and 0.46). On the other hand, the negative correlation between C=C=C signal at 6.37 ppm and total ketone area was weaker ($r = -0.46$). The computed correlations hinted that the molecule producing the signal at 6.37 ppm was able to prevent the formation of aldehydes rather than ketones.

In Fig. 5b, a linear trend can be noticed between the conjugated diene signals at 6.08 and 5.98 ppm and total ketone and total volatile areas. Importantly, there was no overlap between the two, as total ketones had the highest area in only eight samples. On the other hand, the linear trend between the same volatiles and the conjugated diene signals at 6.48 ppm and 6.44 ppm was less evident. The binning of the ^{1}H signals was performed according to their chemical shifts, making mechanistic explanations difficult. It is possible that the lower steric hindrance of an *EE* orientation was more favorable to radical recombination reactions originating ketones or the orientation of a *ZE* conjugated system more favorable to the internal addition of hydroperoxide leading to formation of ketones, as described in Section 3.2.

4. Conclusions

The simulated digestion of *Schizochytrium sp*, cod liver, and rapeseed oils in a HS-SPME-GC-MS apparatus allowed the direct examination in an untargeted manner of volatile compounds produced during gastric and intestinal phases. Such approach, combined with analysis of digesta with other high-throughput methods such as liquid chromatography and

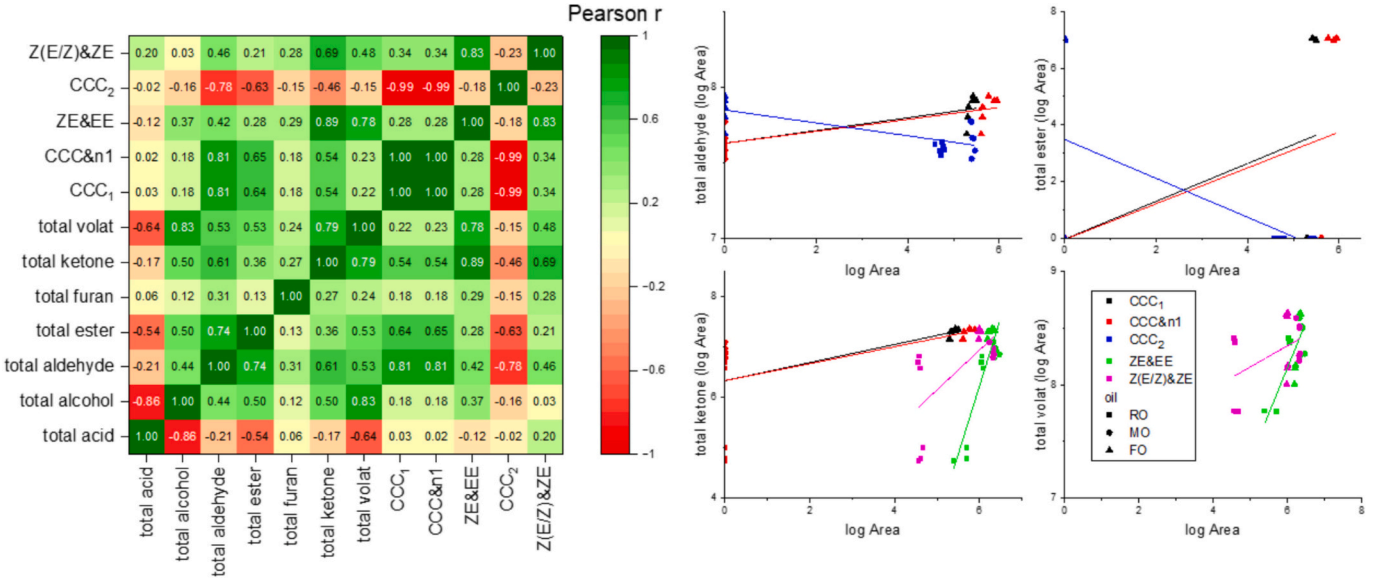

Fig. 5. Heatmap reporting the Pearson correlation between cumulative areas of volatile compound classes and total area of volatiles and ^{1}H area of secondary oxidation products. Most significant correlations between SPME-GC-MS and NMR data are reported as scatter plots with linear fitting to highlight trends.

^{1}H NMR spectroscopy, allowed the detailing of lipid oxidation during simulated digestion even in presence of simulated meal. Despite the complexity of the system and its multiple variables, such as fatty acid composition, presence of antioxidants, and lipolysis, the multivariate analysis of the data discriminated marine oils by the production of n-3 PUFA degradation products, while *Schizochytrium sp* oil was distinguished from the others by volatiles likely originating from terpene degradation. Digestion phases were also discriminated according to specific volatiles. Our results suggested that antioxidants could have contributed to the formation of specific volatiles. While secondary oxidation products were monitored with chromatographic methods, ^{1}H NMR spectroscopy was used to monitor the formation of hydroperoxides. Significant differences (and lack thereof) in the primary oxidation signals between samples highlighted the radical quenching effect of tocopherols and/or terpenes during digestion of *Schizochytrium sp* oil. Finally, the combination of HS-SPME-GC-MS and ^{1}H NMR spectroscopy highlighted correlations between primary oxidation product signals and formation of volatile compounds.

The bioavailability and reactive nature of secondary oxidation products highlights the necessity of detailed analyses of their formation during digestion of oils. The approach reported in the present work, focused on oxidative fate of commercial n-3 PUFA-rich oils, can be applied to outline the oxidative fate of other oils of nutritional relevance. Moreover, it can be utilized to investigate lipid oxidation in the gastrointestinal tract of ingested oils with different degrees of rancidity.

CRediT authorship contribution statement

Gabriele Beltrame: Writing – original draft, Visualization, Investigation, Funding acquisition, Formal analysis, Conceptualization. **Kaisa M. Linderborg:** Writing – review & editing, Supervision, Project administration, Funding acquisition. **Annelie Damerau:** Writing – review & editing, Validation, Methodology, Investigation, Conceptualization, Funding acquisition.

Funding

Personal financial grants to Gabriele Beltrame from the Niemi Foundation and the Finnish Cultural Foundation are acknowledged. Further, personal financial grant to Annelie Damerau from the Finnish Cultural Foundation is acknowledged. This work was carried out as part of the project “Omics of oxidation–Solutions for better quality of docosahexaenoic and eicosapentaenoic acids” funded by the Academy of Finland (grant number 315274, PI Kaisa Linderborg).

Declaration of competing interest

The authors declare that they have no known competing financial interests or personal relationships that could have appeared to influence the work reported in this paper.

Acknowledgments

The authors would like to thank Liisa Hokkanen for her technical help with the SPME-GC-MS experiments and Megan Maher for her technical help with the NMR analysis.

Appendix A. Supplementary data

Supplementary data to this article can be found online at https://doi.org/10.1016/j.foodres.2025.117501.

Data availability

Data will be made available on request.

References

Ahonen, E., Damerau, A., Suomela, J.-P., Kortesniemi, M., & Linderborg, K. M. (2022). Oxidative stability, oxidation pattern and α-tocopherol response of docosahexaenoic acid (DHA, 22:6n–3)-containing triacylglycerols and ethyl esters. *Food Chemistry, 387*, Article 132882. https://doi.org/10.1016/j.foodchem.2022.132882

Aitta, E., Damerau, A., Marsol-Vall, A., Fabritius, M., Pajunen, L., Kortesniemi, M., & Yang, B. (2023). Enzyme-assisted aqueous extraction of fish oil from Baltic herring (Clupea harengus membras) with special reference to emulsion-formation, extraction efficiency, and composition of crude oil. *Food Chemistry, 424*, Article 136381. https://doi.org/10.1016/j.foodchem.2023.136381

Al-Dalali, S., Li, C., & Xu, B. (2022). Effect of frozen storage on the lipid oxidation, protein oxidation, and flavor profile of marinated raw beef meat. *Food Chemistry, 376*, Article 131881. https://doi.org/10.1016/j.foodchem.2021.131881

Beltrame, G., Ahonen, E., Damerau, A., Gudmundsson, H. G., Haraldsson, G. G., & Linderborg, K. M. (2023). Lipid structure influences the digestion and oxidation behavior of docosahexaenoic and Eicosapentaenoic acids in the simulated digestion system. *Journal of Agricultural and Food Chemistry, 71*(26), 10087–10096. https://doi.org/10.1021/acs.jafc.3c02207

Beltrame, G., Damerau, A., Ahonen, E., Mustonen, S. A., Adami, R., Sellitto, M. R., … Linderborg, K. M. (2024). Production and simulated digestion of high-load beads containing *Schizochytrium* oil encapsulated utilizing prilling technique. *Food Chemistry, 460*(P3), Article 140694. https://doi.org/10.1016/j.foodchem.2024.140694

Beltrame, G., Valta, I., Damerau, A., & Linderborg, K. M. (2025). Negative correlation between oil lipolysis and its LC-PUFA content in simulated digestion. *LWT, 224*, Article 117835. https://doi.org/10.1016/j.lwt.2025.117835

Brodkorb, A., Egger, L., Alminger, M., Alvito, P., Assunção, R., Ballance, S., Bohn, T., Bourlieu-Lacanal, C., Boutrou, R., Carrière, F., Clemente, A., Corredig, M., Dupont, D., Dufour, C., Edwards, C., Golding, M., Karakaya, S., Kirkhus, B., Le Feunteun, S., & Recio, I. (2019). INFOGEST static in vitro simulation of gastrointestinal food digestion. *Nature Protocols, 14*(4), 991–1014. https://doi.org/10.1038/s41596-018-0119-1

Colombo, S. M., Rodgers, T. F. M., Diamond, M. L., Bazinet, R. P., & Arts, M. T. (2020). Projected declines in global DHA availability for human consumption as a result of global warming. *Ambio, 49*(4), 865–880. https://doi.org/10.1007/s13280-019-01234-6

Cruz, J. D., & Vasconcelos, V. (2023). Legal aspects of microalgae in the European food sector. *Foods, 13*(1), 124. https://doi.org/10.3390/FOODS13010124

Damerau, A., Ahonen, E., Kortesniemi, M., Puganen, A., Tarvainen, M., & Linderborg, K. M. (2020). Evaluation of the composition and oxidative status of omega-3 fatty acid supplements on the Finnish market using NMR and SPME-GC–MS in comparison with conventional methods. *Food Chemistry, 330*, Article 127194. https://doi.org/10.1016/j.foodchem.2020.127194

Demets, R., & Foubert, I. (2021). Traditional and novel sources of long-chain omega-3 fatty acids. In *Omega-3 Delivery Systems* (pp. 3–23). Elsevier. https://doi.org/10.1016/B978-0-12-821391-9.00013-2.

FAO. (2022). The state of world fisheries and aquaculture 2022. *FAO*. https://doi.org/10.4060/cc0461en

Fiori, L., Solana, M., Tosi, P., Manfrini, M., Strim, C., & Guella, G. (2012). Lipid profiles of oil from trout (Oncorhynchus mykiss) heads, spines and viscera: Trout by-products as a possible source of omega-3 lipids? *Food Chemistry, 134*(2), 1088–1095. https://doi.org/10.1016/J.FOODCHEM.2012.03.022

Frankel, E. (2005). *Lipid oxidation* (2nd ed.). Oily Press.

Frankel, E. N. (1983). Volatile lipid oxidation products. *Progress in Lipid Research, 22*(1), 1–33. https://doi.org/10.1016/0163-7827(83)90002-4

Frétin, M., Gérard, A., Ferlay, A., Martin, B., Buchin, S., Theil, S., … Delbès, C. (2022). Integration of Multiomic data to characterize the influence of Milk fat composition on Cantal-type cheese microbiota. *Microorganisms, 10*(2), 334. https://doi.org/10.3390/microorganisms10020334

Gardner, H. W., Weisleder, D., & Kleiman, R. (1978). Formation of trans-12,13-epoxy-9-hydroperoxy-trans-10-octadecenoic acid from 13-L-hydroperoxy-cis-9,trans-11-octadecadienoic acid catalyzed by either a soybean extract or cysteine-FeC13. *Lipids, 13*(4), 246–252. https://doi.org/10.1007/BF02533664

Grundy, M. M. L., Abrahamse, E., Almgren, A., Alminger, M., Andres, A., Ariëns, R. M. C., … Carrière, F. (2021). INFOGEST inter-laboratory recommendations for assaying gastric and pancreatic lipases activities prior to in vitro digestion studies SUPPLEMENTARY. *Journal of Functional Foods, 82*, Article 104497. https://doi.org/10.1016/j.jff.2021.104497

Hamilton, H. A., Newton, R., Auchterlonie, N. A., & Müller, D. B. (2020). Systems approach to quantify the global omega-3 fatty acid cycle. *Nature Food, 1*(1), 59–62. https://doi.org/10.1038/s43016-019-0006-0

Hammer, M., & Schieberle, P. (2013). Model studies on the key aroma compounds formed by an oxidative degradation of ω-3 fatty acids initiated by either copper(II) ions or lipoxygenase. *Journal of Agricultural and Food Chemistry, 61*(46), 10891–10900. https://doi.org/10.1021/jf403827p

Hennebelle, M., Villeneuve, P., Durand, E., Lecomte, J., van Duynhoven, J., Meynier, A., Yesiltas, B., Jacobsen, C., & Berton-Carabin, C. (2024). Lipid oxidation in emulsions: New insights from the past two decades. *Progress in Lipid Research, 94*, Article 101275. https://doi.org/10.1016/j.plipres.2024.101275

Kakuta, S., Bando, Y., Nishiumi, S., Yoshida, M., Fukusaki, E., & Bamba, T. (2013). Metabolic profiling of oxidized lipid-derived volatiles in blood by gas chromatography/mass spectrometry with in-tube extraction. *Mass Spectrometry, 2*(1), A0018. https://doi.org/10.5702/massspectrometry.A0018

Kimura, T., Takei, Y., & Iida, K. (1984). Mechanisms of adverse effect of air-oxidized soy bean oil-feeding in rats. *Journal of Nutritional Science and Vitaminology, 30*(2), 125–133. https://doi.org/10.3177/JNSV.30.125

Lafountain, A. M., Pacheco, C., Prum, R. O., & Frank, H. A. (2013). Nuclear magnetic resonance analysis of carotenoids from the burgundy plumage of the pompadour Cotinga (Xipholena punicea). *Archives of Biochemistry and Biophysics, 539*(2), 133–141. https://doi.org/10.1016/J.ABB.2013.08.012

Lang, I., Hodac, L., Friedl, T., & Feussner, I. (2011). Fatty acid profiles and their distribution patterns in microalgae: A comprehensive analysis of more than 2000 strains from the SAG culture collection. *BMC Plant Biology, 11*(1), 1–16. https://doi.org/10.1186/1471-2229-11-124/FIGURES/7

Liang, F., Jiang, S., Mo, Y., Zhou, G., & Yang, L. (2015). Consumption of oxidized soybean oil increased intestinal oxidative stress and affected intestinal immune variables in yellow-feathered broilers. *Asian-Australasian Journal of Animal Sciences, 28*(8), 1194–1201. https://doi.org/10.5713/ajas.14.0924

Lorrain, B., Dangles, O., Loonis, M., Armand, M., & Dufour, C. (2012). Dietary iron-initiated lipid oxidation and its inhibition by polyphenols in gastric conditions. *Journal of Agricultural and Food Chemistry, 60*(36), 9074–9081. https://doi.org/10.1021/JF302348S/ASSET/IMAGES/LARGE/JF-2012-02348S_0006.JPEG

Martínez-Yusta, A., Goicoechea, E., & Guillén, M. D. (2014). A review of thermo-oxidative degradation of food lipids studied by 1H NMR spectroscopy: Influence of degradative conditions and food lipid nature. *Comprehensive Reviews in Food Science and Food Safety, 13*(5), 838–859. https://doi.org/10.1111/1541-4337.12090

Martini, S., Cavalchi, M., Conte, A., & Tagliazucchi, D. (2018). The paradoxical effect of extra-virgin olive oil on oxidative phenomena during in vitro co-digestion with meat. *Food Research International, 109*(March), 82–90. https://doi.org/10.1016/j.foodres.2018.04.031

Micha, R., Khatibzadeh, S., Shi, P., Fahimi, S., Lim, S., Andrews, K. G., … Mozaffarian, D. (2014). Global, regional, and national consumption levels of dietary fats and oils in 1990 and 2010: A systematic analysis including 266 country-specific nutrition surveys. *The BMJ, 348*(April), 1–20. https://doi.org/10.1136/bmj.g2272

Morabito, C., Bournaud, C., Maës, C., Schuler, M., Aiese Cigliano, R., Dellero, Y., Maréchal, E., Amato, A., & Rébeillé, F. (2019). The lipid metabolism in thraustochytrids. *Progress in Lipid Research, 76*, Article 101007. https://doi.org/10.1016/J.PLIPRES.2019.101007

Nieva-Echevarría, B., Goicoechea, E., & Guillén, M. D. (2017). Polyunsaturated lipids and vitamin a oxidation during cod liver oil in vitro gastrointestinal digestion. Antioxidant effect of added BHT. *Food Chemistry, 232*, 733–743. https://doi.org/10.1016/J.FOODCHEM.2017.04.057

Nieva-Echevarría, B., Goicoechea, E., & Guillén, M. D. (2020). Food lipid oxidation under gastrointestinal digestion conditions: A review. *Critical Reviews in Food Science and Nutrition, 60*(3), 461–478. https://doi.org/10.1080/10408398.2018.1538931

Rietjens, I. M. C. M., Boersma, M. G., de, H., .L., Spenkelink, B., Awad, H. M., Cnubben, N. H. P., … Koeman, J. H. (2002). The pro-oxidant chemistry of the natural antioxidants vitamin C, vitamin E, carotenoids and flavonoids. *Environmental Toxicology and Pharmacology, 11*(3–4), 321–333. https://doi.org/10.1016/S1382-6689(02)00003-0

Rogalska, E., Ransac, S., & Verger, R. (1990). Stereoselectivity of lipases. II. Stereoselective hydrolysis of triglycerides by gastric and pancreatic lipases. *Journal of Biological Chemistry, 265*(33), 20271–20276. https://doi.org/10.1016/s0021-9258(17)30500-8

RStudio.. (2020). *RStudio: Integrated development for R*. Boston, MA: RStudio, Inc. http://www.rstudio.com/.

Sabet, S., Kirjoranta, S. J., Lampi, A.-M., Lehtonen, M., Pulkkinen, E., & Valoppi, F. (2022). Addressing criticalities in the INFOGEST static in vitro digestion protocol for oleogel analysis. *Food Research International, 160*, Article 111633. https://doi.org/10.1016/J.FOODRES.2022.111633

Sabikun, N., Bakhsh, A., Rahman, M. S., Hwang, Y.-H., & Joo, S.-T. (2021). Volatile and nonvolatile taste compounds and their correlation with umami and flavor characteristics of chicken nuggets added with milkfat and potato mash. *Food Chemistry, 343*, Article 128499. https://doi.org/10.1016/j.foodchem.2020.128499

Saini, R. K., & Keum, Y. S. (2018). Omega-3 and omega-6 polyunsaturated fatty acids: Dietary sources, metabolism, and significance — A review. *Life Sciences, 203*, 255–267. https://doi.org/10.1016/j.lfs.2018.04.049

Schaich, K. M. (2020). Toxicity of lipid oxidation products consumed in the diet. In *Bailey's industrial oil and fat products* (pp. 1–88). Wiley. https://doi.org/10.1002/047167849X.bio116.

Shepon, A., Makov, T., Hamilton, H. A., Müller, D. B., Gephart, J. A., Henriksson, P. J. G., … Golden, C. D. (2022). Sustainable optimization of global aquatic omega-3 supply chain could substantially narrow the nutrient gap. *Resources, Conservation and Recycling, 181*, Article 106260. https://doi.org/10.1016/j.resconrec.2022.106260

Shimizu, N., Ito, J., Kato, S., Otoki, Y., Goto, M., Eitsuka, T., Miyazawa, T., & Nakagawa, K. (2018). Oxidation of squalene by singlet oxygen and free radicals results in different compositions of squalene monohydroperoxide isomers. *Scientific Reports, 8*(1), 9116. https://doi.org/10.1038/s41598-018-27455-5

Sommerburg, O., Langhans, C.-D., Arnhold, J., Leichsenring, M., Salerno, C., Crifò, C., … Siems, W. G. (2003). B-Carotene cleavage products after oxidation mediated by hypochlorous acid—A model for neutrophil-derived degradation. *Free Radical Biology and Medicine, 35*(11), 1480–1490. https://doi.org/10.1016/j.freeradbiomed.2003.08.020

Tan, Y., Zhang, Z., Zhou, H., Xiao, H., & McClements, D. J. (2020). Factors impacting lipid digestion and β-carotene bioaccessibility assessed by standardized gastrointestinal model (INFOGEST): Oil droplet concentration. *Food & Function, 11*(8), 7126–7137. https://doi.org/10.1039/D0FO01506G

Thévenot, E. A., Roux, A., Xu, Y., Ezan, E., & Junot, C. (2015). Analysis of the human adult urinary metabolome variations with age, body mass index, and gender by implementing a comprehensive workflow for univariate and OPLS statistical analyses. *Journal of Proteome Research, 14*(8), 3322–3335. https://doi.org/10.1021/ACS.JPROTEOME.5B00354/SUPPL_FILE/PR5B00354_SI_003.ZIP

Tocher, D. R., Betancor, M. B., Sprague, M., Olsen, R. E., & Napier, J. A. (2019). Omega-3 long-chain polyunsaturated fatty acids, EPA and DHA: Bridging the gap between supply and demand. In *, Vol. 11, Issue 1. Nutrients* (p. 89). Multidisciplinary Digital Publishing Institute. https://doi.org/10.3390/nu11010089.

Tullberg, C., & Undeland, I. (2021). Oxidative stability during digestion. In *Omega-3 Delivery Systems* (pp. 449–479). Elsevier. https://doi.org/10.1016/B978-0-12-821391-9.00008-9.

Tullberg, C., Vegarud, G., & Undeland, I. (2019). Oxidation of marine oils during in vitro gastrointestinal digestion with human digestive fluids – Role of oil origin, added tocopherols and lipolytic activity. *Food Chemistry, 270*(May 2018), 527–537. https://doi.org/10.1016/j.foodchem.2018.07.049

Van Hecke, T., Wouters, A., Rombouts, C., Izzati, T., Berardo, A., Vossen, E., … De Smet, S. (2016). *Reducing compounds equivocally influence oxidation during digestion of*

a high-fat beef product, which promotes cytotoxicity in colorectal carcinoma cell lines. https://doi.org/10.1021/acs.jafc.5b05915

Vieira, S. A., Zhang, G., & Decker, E. A. (2017). Biological implications of lipid oxidation products. *Journal of the American Oil Chemists' Society, 94*(3), 339–351. https://doi.org/10.1007/s11746-017-2958-2

Zhou, H., Tan, Y., & McClements, D. J. (2023). Applications of the INFOGEST in vitro digestion model to foods: A review. *Annual Review of Food Science and Technology, 14*(1), 135–156. https://doi.org/10.1146/annurev-food-060721-012235